

## Article

# Mechanistic Insights into the Effect of Sulfur on the Selectivity of Cobalt-Catalyzed Fischer–Tropsch Synthesis: A DFT Study

Yagmur Daga and Ali Can Kizilkaya \* 

Department of Chemical Engineering, Izmir Institute of Technology, Urla, Izmir 35430, Turkey; yagmur.daga@gmail.com

\* Correspondence: alicankizilkaya@iyte.edu.tr

**Abstract:** Sulfur is a common poison for cobalt-catalyzed Fischer–Tropsch Synthesis (FTS). Although its effects on catalytic activity are well documented, its effects on selectivity are controversial. Here, we investigated the effects of sulfur-covered cobalt surfaces on the selectivity of FTS using density functional theory (DFT) calculations. Our results indicated that sulfur on the surface of Co(111) resulted in a significant decrease in the adsorption energies of CO, HCO and acetylene, while the binding of H and CH species were not significantly affected. These findings indicate that sulfur increased the surface H/CO coverage ratio while inhibiting the adsorption of carbon chains. The elementary reactions of H-assisted CO dissociation, carbon and oxygen hydrogenation and CH coupling were also investigated on both clean and sulfur-covered Co(111). The results indicated that sulfur decreased the activation barriers for carbon and oxygen hydrogenation, while increasing the barriers for CO dissociation and CH coupling. Combining the results on elementary reactions with the modification of adsorption energies, we concluded that the intrinsic effect of sulfur on the selectivity of cobalt-catalyzed FTS is to increase the selectivity to methane and saturated short-chain hydrocarbons, while decreasing the selectivity to olefins and long-chain hydrocarbons.

**Keywords:** sulfur; cobalt; Fischer–Tropsch Synthesis; selectivity; density functional theory



**Citation:** Daga, Y.; Kizilkaya, A.C. Mechanistic Insights into the Effect of Sulfur on the Selectivity of Cobalt-Catalyzed Fischer–Tropsch Synthesis: A DFT Study. *Catalysts* **2022**, *12*, 425. <https://doi.org/10.3390/catal12040425>

Academic Editors: Maria Jaworska and Piotr Lodowski

Received: 24 March 2022

Accepted: 8 April 2022

Published: 10 April 2022

**Publisher's Note:** MDPI stays neutral with regard to jurisdictional claims in published maps and institutional affiliations.



**Copyright:** © 2022 by the authors. Licensee MDPI, Basel, Switzerland. This article is an open access article distributed under the terms and conditions of the Creative Commons Attribution (CC BY) license (<https://creativecommons.org/licenses/by/4.0/>).

## 1. Introduction

Sulfur is widely regarded as a catalyst poison in Fischer–Tropsch Synthesis (FTS) [1]. Nevertheless, the effects of sulfur on the selectivity of FTS are not well understood. Recent studies on cobalt-catalyzed FTS promoted with Mn, Na and S have shown that the selectivity can be altered significantly [2], highlighting the potential of sulfur in selectivity modification. Although the effects of S on the selectivity of Co-catalyzed FTS have been subject to various experimental investigations [3–7], the reported findings typically show a complex effect of S on product selectivity and often contradict with each other, making the conclusions controversial.

Earlier studies performed by in situ poisoning (the introduction of sulfur-containing compounds via feed lines) of cobalt FTS catalysts have indicated that sulfur induces an increase in the selectivity of long-chain hydrocarbons, while methane selectivity is mainly unaffected [3]. In contrast, later studies based on ex situ poisoning (the addition of sulfur during catalyst synthesis) have indicated that sulfur decreases the selectivity to heavier hydrocarbons, while increasing methane selectivity [4,7]. Visconti et al. studied the effect of ex situ sulfur poisoning in the range of 0–2000 ppmw on an alumina-supported Co catalyst [4]. The authors reported that sulfur increased the selectivity to methane, light products (C<sub>2</sub>–C<sub>5</sub>) and olefins, in contrast to a decreased selectivity for heavier (C<sub>5+</sub> and C<sub>25+</sub>) products. However, the authors mentioned that while for paraffins, C<sub>2</sub>–C<sub>5</sub> selectivity increased and C<sub>5+</sub> selectivity decreased continuously with increased S loading, the selectivity for olefins increased to a maximum before decreasing with the highest S loading. It was also proposed that the varying effects of sulfur on the selectivity of different

products could be due to the distinct effects of sulfur on active sites that catalyze CO hydrogenation and chain growth processes. As low levels of sulfur addition resulted in negligible changes in selectivity, while higher levels resulted in major changes, the authors concluded that sulfur poisoning of cobalt is selective poisoning, meaning that sulfur preferentially adsorbs on the most active sites involved in FTS. The authors also speculated that the changes in selectivity may be related to the formation of cobalt sulfide. In a later study, Borg et al. [5] studied the effect of in situ H<sub>2</sub>S exposure on an alumina-supported cobalt-based catalyst. Although the results showed that C<sub>5+</sub> selectivity decreased with increasing sulfur concentration, the changes in selectivity were similar for increasing CO conversion with a sulfur-free catalyst. Therefore, the authors concluded that sulfur did not affect FTS selectivity.

The influence of in situ sulfur addition, in the form of dimethyl sulfide, on the selectivity of Co-catalyzed FTS was investigated by Pansare and Allison [6]. The authors observed that sulfur decreased the selectivity to both C<sub>5+</sub> and olefins, while increasing the selectivity to methane. They speculated that this could be due to the decreased H<sub>2</sub> and CO coverage, which could be a result of either site blocking or changes in the electronic charge induced by the adsorbed sulfur. The authors proposed that the formation of cobalt sulfide on the catalyst could result in the promotion of hydrogenation reactions, while inhibiting chain growth. In a recent study by Barrientos et al. [7], ex situ sulfur-poisoned alumina-supported cobalt catalysts were tested under the same CO conversion. The authors reported that the selectivities to methane and C<sub>2</sub>–C<sub>4</sub> products increased with an increasing sulfur amount, while the selectivity to heavier (C<sub>5+</sub>) hydrocarbons decreased. The authors found out that although the overall C<sub>2</sub>–C<sub>4</sub> selectivity increased, the olefin-to-paraffins ratio decreased for this carbon number range. Therefore, they concluded that sulfur increased the secondary hydrogenation of olefins. The authors also suggested that these observed effects may be due the formation of cobalt sulfide.

Among the various reasons for the contradicting results obtained by these experimental studies are differences in the introduction of sulfur to the catalyst surface (in situ vs. ex situ), intra-particle and reactor concentration gradients and ambiguities in sulfur adsorption stoichiometry and the modified cobalt surface morphology and electronic structure resulting from sulfur adsorption. Furthermore, it is not clear from these studies, whether sulfur poisons the catalyst through a site-blocking or electronic effect, or how sulfur effects the adsorption of different adsorbates on cobalt surfaces in terms of their adsorption energies, sites and surface coverages. These fundamental questions can be answered via surface science studies on well-defined cobalt surfaces, or molecular modeling studies utilizing density functional theory (DFT) calculations.

There are limited number of studies that have approached the issue from this fundamental perspective by the experimental investigation of Co(0001) single crystal surfaces [8–11]. Habermehl-Cwirzen et al. investigated the adsorption of D<sub>2</sub> [9] and CO [10] on S-covered Co(0001) surfaces using a combination of low energy electron diffraction (LEED), X-ray photoelectron spectroscopy (XPS), thermal desorption spectra (TDS) and work function (WF) measurements. The authors reported that [9] after the exposure of the surface to H<sub>2</sub>S as a sulfur source and annealing to 650 K, adsorbed atomic sulfur (S<sub>ad</sub>) was obtained on the surface. The saturation coverage of S<sub>ad</sub> was determined as 0.25 ML and a p(2 × 2) ordered structure was observed by LEED at this coverage [10]. Furthermore, no surface reconstruction was observed at this coverage. By a combination of LEED and DFT calculations, another study reported [8] that sulfur adsorbed on hollow sites, while the fcc and hcp types of hollow sites were energetically similar. It was suggested that sulfur withdraws electronic charge from the cobalt surface and a strong hybridization occurs between the Co-d and S-p states, resulting in the strong adsorption of sulfur in hollow sites on the Co(0001) surface. They proposed that this additional charge on adsorbed sulfur could result in different adsorbates binding to sulfur.

For the effect of sulfur on hydrogen adsorption, it was reported in [9] that S<sub>ad</sub> decreased the desorption temperature of D<sub>2</sub> from 400 to 300 K, indicating the destabilization of

adsorbed deuterium as a result of sulfur coadsorption. It was also found that no deuterium adsorption took place on Co(0001) at a sulfur coverage of 0.25 ML, which the authors proposed could be due to the site-blocking effect of sulfur. For CO adsorption, it was found in [10] that CO could still adsorb on Co(0001) surfaces covered by 0.25 ML  $S_{ad}$ , and each S atom blocked 1.2 sites for CO, effectively halving the CO coverage that could be accommodated on the surface. For low S coverages, such as 0.11 ML, CO was assumed to occupy only the top sites, while for 0.25 ML  $S_{ad}$  coverage, CO was found to occupy both the top and hollow sites. At this  $S_{ad}$  coverage, the CO adsorption energy was found to decrease from 113 to 66 kJ/mol for 0.25 ML  $S_{ad}$ , while it decreased marginally from 113 to 111 kJ/mol for 0.11 ML  $S_{ad}$ . It was proposed that the reduction in CO adsorption energy could stem from the smaller back-donation to the CO molecule from the surface atoms, due to the electron-withdrawing sulfur atoms. It was also found that on both clean and  $S_{ad}$ -covered Co(0001), CO underwent molecular desorption, ruling out direct CO dissociation in both cases.

A recent in situ STM study [11] performed on Co(0001) under 10 mbar syngas pressure and 500 K investigated the changes in the surface structure as a result of sulfur poisoning and subsequent syngas exposure. The decrease in methanation activity was related to the formation of an adsorbed sulfur layer on the cobalt surface, where the formation of bulk cobalt sulfide was ruled out based on XPS measurements. STM images showed that while the use of sulfur-free syngas resulted in atomic terraces of 100 Å, sulfur-containing syngas resulted in the reconstruction of the surface to smaller terraces of around 10 Å in size. The authors concluded that the reconstructed surface that formed after sulfur-containing syngas exposure involved a mixed phase of S and C adatoms. STM and XPS measurements confirmed that atomic sulfur formed  $p(2 \times 2)$  ordered structures, while the sulfur coverage on the surface varied between 0.23 ML and 0.41 ML for hydrogen only and syngas atmospheres, respectively. Based on the evidence that sulfur deposits were observed at terraces after syngas exposure, the authors concluded that sulfur poisoning follows a non-selective mechanism, meaning that sulfur adsorbs at both undercoordinated and terrace sites, resulting in the poisoning effect. Besides the fact that these surface science studies provide valuable insights related to the fundamentals of sulfur poisoning of cobalt surfaces, they do not provide answers related to how the  $S_{ad}$  layer formed on cobalt surfaces affects the selectivity of FTS.

There are a few studies that have investigated the sulfur poisoning of metal surfaces with DFT calculations. McAllister and Hu [12] investigated  $H_2S$  decomposition on Rh(111) and Rh(211) surfaces, and concluded that sulfur adsorbed more strongly on Rh(211) steps compared to Rh(111) terraces. The authors also concluded that the hydrogenation of atomic S to  $H_2S$  was significantly slower compared to the hydrogenation of atomic C and O, and they proposed that this finding could account for the poisoning effect of S on Rh surfaces. Curulla-Ferre et al. [13] investigated how  $S_{ad}$  effects the adsorption and direct dissociation of CO on an Fe(100) surface. They reported that coadsorption with S resulted in varying decreases in the adsorption energy of CO, ranging from 25 to 150 kJ/mol, based on the CO adsorption site and S coverage. The activation barrier for direct CO dissociation increased by 15 kJ/mol on S-covered Fe(100) compared to the clean surface, while S changed the exothermic CO dissociation to an endothermic reaction. On cobalt surfaces, Ma et al. [14] investigated how sulfur adsorption energy and site preference changed on Co(0001) as a function of coverage up to 1 ML, and concluded that sulfur occupied the fcc sites for all coverages investigated, while sulfur adsorption became stronger going from 0.11 ML to 0.25 ML, whereas above 0.25 ML it became weaker with increasing coverage. To the best of our knowledge, there are no computational studies investigating the effect of sulfur on the performance of cobalt-catalyzed FTS.

The aim of this study was to investigate how sulfur adsorbed on cobalt surfaces effects the selectivity of FTS, based on DFT modeling. In order to answer this question, first, the effects of sulfur on adsorption sites and the energies of various reactants and surface species involved in FTS were calculated on Co(111) surfaces covered with 0.25 ML  $S_{ad}$

corresponding to a  $p(2 \times 2)$  periodic structure—the only experimentally observed periodic structure for sulfur-poisoned cobalt surfaces [10,11]. Afterwards, the effects of sulfur on the main elementary reactions of FTS were investigated. As the exact mechanism of FTS is under debate, assuming a specific mechanism may lead to results that are restricted to only the studied mechanism. However, fundamentally, it can be concluded that a cobalt FTS catalyst must be active in four types of main reactions, which are CO dissociation, carbon hydrogenation, oxygen hydrogenation and carbon coupling [15]. Therefore, in this study, we investigated the effects of sulfur on the mentioned elementary reactions. Furthermore, we studied the effect of 0.11 ML and 0.06 ML sulfur coverages on adsorbates on Co(111) in order to compare the effects of different sulfur coverages. Our results indicate that sulfur results in cobalt surfaces with increased H and decreased CO coverage by the modification of adsorption energies, and it promotes hydrogenation reactions over carbon coupling while inhibiting H-assisted CO dissociation. Our study provides an example of how a catalyst poison can affect the complex reaction mechanism on a catalyst surface.

## 2. Computational Methodology

### 2.1. Computational Model

To investigate the effect of sulfur on the surfaces of fcc cobalt nanoparticles, atomic sulfur adsorbed ( $S_{ad}$ ) on Co(111) surfaces was used as a model with a  $p(2 \times 2)$  unit cell, corresponding to a sulfur coverage of 0.25 ML. The selection of this model and coverage was based on experiments performed on cobalt single crystal surfaces under vacuum, hydrogen and syngas exposure and supported cobalt nanoparticles under applied FTS conditions. Experimental surface science studies under vacuum conditions have indicated that  $H_2S$  readily decomposes to atomic S on Co(0001), forming a  $p(2 \times 2)$  structure at a sulfur saturation coverage of 0.25 ML [10]. The formation of chemisorbed sulfur on metallic cobalt terraces, instead of cobalt sulfide, with coverages between 0.23 ML and 0.41 ML and in  $p(2 \times 2)$  periodic structures was also observed in a recent in situ STM study, which investigated the poisoned state of the catalyst after sulfur-containing hydrogen and syngas exposure at conditions of  $P = 10$  mbar and  $T = 500$  K [11]. The study also confirmed that the  $p(2 \times 2)$  structure is the only experimentally observed ordered structure for chemisorbed sulfur on cobalt surfaces. These experimental studies [10,11] showed that sulfur forms  $p(2 \times 2)$  ordered structures resulting in a local surface coverage of 0.25 ML under vacuum, hydrogen and syngas atmospheres, providing solid support for the selection of our model of chemisorbed sulfur atoms with  $p(2 \times 2)$  periodicity, corresponding to 0.25 ML sulfur coverage.

Other experimental studies [6,7] have also attempted to calculate surface coverage based on inductively coupled plasma mass spectrometry (ICP-MS) data for sulfur uptake and activity loss data as a function of sulfur loading. These experimental studies performed with applied FTS conditions on supported cobalt nanoparticles indicated that the sulfur coverage at which the activity loss was 100% was around 0.6 ML. These studies also indicated that high (0.25 ML and higher) sulfur coverages were possible on the sulfur-poisoned cobalt nanoparticle surfaces, and the selectivity modification was more pronounced starting from sulfur coverages of 0.1 ML [7] and 0.2 ML [6]. Therefore, these experimental studies on cobalt single crystal surfaces and supported cobalt nanoparticles provide evidence that ordered chemisorbed sulfur with  $p(2 \times 2)$  periodicity and 0.25 ML coverage is a suitable model to study the effects of sulfur poisoning on the selectivity of cobalt-catalyzed FTS. The total surface coverages of 0.5 ML in the case of sulfur coadsorption with a single reactant/product and 0.75 ML in the case of sulfur coadsorption with two types of surface species (e.g.,  $S\_C\_H$  coadsorption) structures are also reasonable, as such total coverages have been reported in both sulfur-poisoned [6,7,11] and clean cobalt surfaces [15,16] under FTS conditions. Furthermore, in order to investigate the effect of coverages lower than 0.25 ML,  $p(3 \times 3)$  and  $p(4 \times 4)$  unit cells were used in this study to investigate the effects of lower sulfur coverages of 0.11 ML and 0.06 ML, respectively.

The fcc cobalt polymorph was used as model as it has been reported to be the most stable phase in cobalt nanoparticles with sizes below 110 nm [16]. Fcc Co nanoparticles preferentially adopt a regular truncated octahedron shape and expose predominantly close-packed (111) terraces and undercoordinated sites, such as step-edges or kinks. Although it is of interest to investigate the interaction of sulfur with the undercoordinated sites on a cobalt nanoparticle, such as steps or kinks, it has been reported that after FTS operation on a Co(0001) single crystal surface, the surface reconstructs into small terraces that are covered by  $S_{ad}$  [11]. Furthermore, it has also been reported that step sites on a cobalt nanoparticle are at low concentrations and can already be covered by atomic C or O species [15], and the kinetically relevant steps together with chain formation possibly occur on terraces of cobalt nanoparticles [17]. Therefore, it is of interest to investigate how atomic sulfur on Co(111) terraces affects the adsorption energies of surface species and the reaction parameters (activation barriers and reaction energies) of elementary reactions to elucidate the effect of sulfur on the selectivity of Co-catalyzed FTS.

## 2.2. Computational Details

Periodic density functional calculations were performed using the Vienna Ab-initio simulation package (VASP) [17,18]. The exchange–correlation energy was calculated with the revised Perdew–Burke–Ernzerhof functional (revPBE) [19] including the non-local vdW–DF correlation [20–23]. The use of the vdW-DF functional allowed us to predict the experimentally observed adsorption site and energy for adsorbed CO on the cobalt surface [24]. The surfaces were cut from a bulk fcc-Co structure with a lattice parameter of 3.56 Å, optimized with the vdW-DF functional. The calculated lattice parameter matched very well with the experimental value of 3.55 Å [25] and the value of 3.56 Å calculated in a recent DFT study on a Co(111) surface using the same vdW-DF functional [26].

The electron–ion interaction was modeled using the projector-augmented wave (PAW) method. Spin-polarized calculations were performed to account for the magnetic properties of cobalt with a plane wave cut-off energy of 600 eV. A further increase in the cut-off energy resulted in less than 1 kJ/mol difference in the CO adsorption energy. The surface terraces of face-centered cubic (fcc) Co nanoparticles were modeled with Co(111) slabs that were 4 atomic layers thick with  $p(2 \times 2)$ ,  $p(3 \times 3)$  and  $p(4 \times 4)$  unit cells. The number of layers was determined based on the minimization of the surface energy as a function of the number of layers. The surface energy was calculated for slabs containing 3, 4 and 5 layers according to the following equation:

$$E_{surf} = 0.5 * (E_{slab} - N_{atoms} * E_{bulk}) \quad (1)$$

where  $E_{surf}$  is the surface free energy,  $E_{slab}$  is the energy of the optimized slab,  $N_{atoms}$  is the number of Co atoms in the calculated slab and  $E_{bulk}$  is the energy obtained as a result of the bulk optimization of the fcc-Cobalt. Furthermore, the increase in the number of layers from 4 to 5 resulted in less than 3 kJ/mol difference in the adsorption energy of CO.

The atoms at the bottom 2 layers of the slabs in the  $z$ -direction were kept fixed at their pre-optimized positions, while all other atoms, including sulfur, were allowed to relax during the optimization calculations. The reciprocal space was sampled with a  $(5 \times 5 \times 1)$ ,  $(3 \times 3 \times 1)$  and  $(2 \times 2 \times 1)$   $k$ -points grid for  $p(2 \times 2)$ ,  $p(3 \times 3)$  and  $p(4 \times 4)$  unit cells, respectively, which were automatically generated using the Monkhorst–Pack method [27]. The number of  $k$ -points for the different sized unit cells were based on the scaling of the optimized  $k$ -points number of 17 for the bulk fcc-Cobalt structure. A vacuum height of 15 Å was inserted between slabs to avoid coupling between successive slabs in the  $z$ -direction. The vacuum height used was sufficient as increasing the vacuum height to 20 Å did not result in a change in the CO adsorption energy. The structural models were optimized until all the forces acting on the atoms were smaller than 0.02 eV/Å. Dipole corrections in the  $z$ -direction were used for all optimizations.

The binding (adsorption) energies ( $E_{ad}$ ) of surface species (adsorbates) were reported with respect to their gas-phase structures, according to the following formula:

$$E_{ad} = E_{slab\_ad} - E_{slab} - E_{ad\_vac} \quad (2)$$

where  $E_{slab\_ad}$  represents the energy of the optimized system of adsorbate on the slab,  $E_{slab}$  represents the energy of the clean slab (without the adsorbate) and  $E_{ad\_vac}$  represents the energy of the adsorbate molecule in a vacuum.

The lateral interactions between adsorbed sulfur atoms were calculated based on the sulfur adsorption energies for the investigated coverages. As the difference in sulfur adsorption energy was less than 10 kJ/mol between all three coverages investigated, and the highest adsorption energy (i.e., the strongest adsorption for sulfur) was obtained for the  $p(2 \times 2)$  unit cell, it was concluded that the lateral repulsion between S atoms was not significant between 0.06 ML and 0.25 ML. This result was also in line with previous DFT calculations of sulfur adsorption on Co(0001) indicating that the sulfur adsorption becomes stronger as the coverage is increased from 0.11 to 0.25 ML [14], and also in line with the experimental observations that the  $p(2 \times 2)$  structure is the only stable periodic structure on cobalt surfaces [10,11]. The top and side views of S-covered Co(111) in a  $p(2 \times 2)$  unit cell are provided in Supporting Information, Figure S11.

The effect of zero-point energies (ZPEs) on the adsorption energies of surface species and reaction parameters was tested for the adsorption of  $CH_4$  and the elementary reaction of  $CH_4$  formation from  $CH_{3ad}$  and  $H_{ad}$ . It has been reported in the literature that the inclusion of ZPEs effects the results more significantly for species with a higher number of H-bonds, such as  $CH_4$  [28]. The calculations indicated that the change in the adsorption energy for  $CH_4$  was zero for both bare and S-Co(111), and the change in the activation barrier for  $CH_4$  formation was 9 and 16 kJ/mol on bare and S-Co(111), respectively; therefore, the adsorption energy was not effected and the change in the activation barrier for  $CH_4$  formation due to sulfur compared to bare Co(111) was effected by 7 kJ/mol by the inclusion of ZPEs. As  $CH_4$  is the species that would be effected most by the inclusion of ZPEs, and since the aim of this study was to compare the changes in the adsorption energies of surface species and the reaction parameters of elementary reactions due to presence of sulfur on Co(111), ZPEs were not included in the results as they did not change the conclusions drawn in our work. Bader analysis [29–31] was performed to investigate changes in electronic charge on adsorbates on both clean and  $S_{ad}$ -covered Co(111) surfaces. The activation barriers were calculated based on the optimized transition states for each elementary reaction. The transition states were optimized using the CI-NEB [32] method until the forces acting on the image with the highest energy were lower than 0.04 eV/Å. All transition states were further confirmed by vibrational frequency analysis, which indicated a single imaginary vibrational frequency. During the vibrational frequency analysis, the atoms were displaced from their equilibrium positions by 0.015 Å.

### 3. Results and Discussion

#### 3.1. Effect of Sulfur on the Adsorption of the Reactants and Intermediates of FTS on Co(111)

The adsorption of atomic sulfur was investigated for the four different possible adsorption sites: the top, bridge, fcc and hcp sites. Of the investigated adsorption sites, the calculations started from initial guesses of the top and bridge sites converged to sulfur adsorbed at fcc and hcp sites, respectively. The  $E_{ad}$  values for sulfur at the fcc and hcp sites were calculated as 491 and 490 kJ/mol, respectively, indicating that the fcc site was slightly more preferred for  $S_{ad}$  compared to the hcp site. The site preference of  $S_{ad}$  is consistent with previous DFT investigations of sulfur on Co(0001) surfaces [8,14]. The calculated adsorption energy was lower compared to 535 [10] and 527 [14] kJ/mol, reported in studies using the PBE functional. This is as a result of the PBE functional overestimating the adsorption energy compared to the vdW-functional used in our study, which produces adsorption energies that are more consistent with the experimental measurements [25].

The adsorption structures for the surface species on Co(111) surfaces covered with  $S_{ad}$  (S-Co(111)) are given in Figure 1.

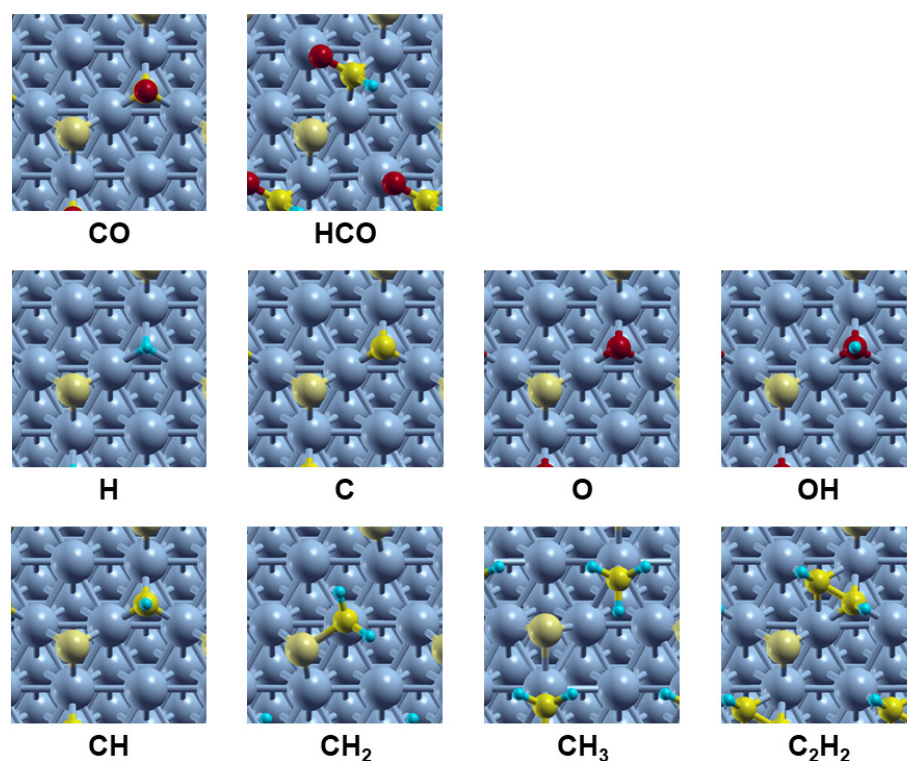


**Figure 1.** Adsorption sites for various adsorbates on the surface of  $p(2 \times 2)$ -S-Co(111). Color coding: sulfur—pale yellow; C—bright yellow; O—red; H—blue; Co—grey.

As seen in Figure 1, in the coadsorption structures, sulfur kept its preferred adsorption site of fcc. For surface species coadsorbed with  $S_{ad}$ , CO and HCO were displaced from their preferred adsorption sites of top and hcp on clean Co(111) to the hcp and fcc sites on S-Co(111). It is worthwhile to mention that  $CH_2$  stayed bonded to the  $S_{ad}$  while  $CH_3$  was bound to the same Co atom with S, for their coadsorption structures on S-Co(111). This finding is line with the predictions made in the experimental literature that  $S_{ad}$  may act as an adsorption site due to the additional charge it accumulates on cobalt terraces [10]. The changes in adsorption sites and energies for the surface species due to coadsorption with  $S_{ad}$  on Co(111) are tabulated in Table 1.

**Table 1.** Adsorption sites and energies (kJ/mol) for adsorbates on Co(111) vs. S-Co(111) surfaces.

	Co(111)		S-Co(111)		$\Delta E_{ad}$ (%)
	Energy	Adsorption Site	Energy	Adsorption Site	
CO	−140	top	−70	hcp	−50
HCO	−194	hcp	−87	fcc	−55
H	−288	fcc	−262	hcp	−9
C	−647	hcp	−562	hcp	−13
CH	−635	hcp	−600	hcp	−6
$CH_2$	−414	fcc	−342	top	−17
$CH_3$	−229	fcc	−117	top	−49
$CH_4$	−22	top	−24	top	9
$C_2H_2$	−206	hcp and fcc	−6	hcp and fcc	−97
O	−545	hcp	−451	hcp	−7
OH	−385	hcp	−288	hcp	−25
$H_2O$	−28	top	−25	top	−11

Table 1 shows that  $S_{ad}$  decreased the adsorption energies of all the chemisorbed surface species and  $H_2O$  (physisorbed) on Co(111). For  $CH_4$ , there was a slight increase in  $E_{ad}$ . However, as the  $E_{ad}$  for  $CH_4$  was below 30 kJ/mol on both clean and sulfur-covered Co(111), the increases in  $E_{ad}$  were not significant, as both cases represented physisorption and the molecules were located far from the surface in the direction of vacuum. The adsorption energies on clean Co(111) are in qualitative agreement with the values in the literature, as shown in Table S1. In general, the adsorption energies were lower in this study, as the vdW-dF functional used in our study results in values that are more consistent with the experimental results [24], while the PBE functional, used in the compared literature [25,33,34], results in the overestimation of adsorption energies.

For the chemisorbed species, although the  $E_{ad}$  decreased for adsorption on S-Co(111), the magnitude of decrease varied significantly for different species. The highest decrease was observed for acetylene ( $C_2H_2$ ), where the adsorption energy decreased to  $-6$  kJ/mol, with a 97% decrease for S-Co(111) compared to Co(111). For CO and HCO,  $E_{ad}$  decreased by 50 and 55% respectively. For these species, sulfur also induced a change in the preferred adsorption site, which contributed to the major drop in  $E_{ad}$ . For CO, the top adsorption site and  $-140$  kJ/mol  $E_{ad}$  are consistent with the experimentally reported on-top adsorption of CO on Co(0001) with an  $E_{ad}$  of  $-128$  kJ/mol, and with the  $E_{ad}$  of  $-135$  kJ/mol obtained by a DFT study that utilized the vdW-dF functional [25] for 0.33 ML CO coverage on Co(0001). The preferred adsorption site of CO shifted from top to hcp in the case of coadsorption with CO, which was also speculated based on the XPS binding energies for CO adsorption on 0.25 ML  $S_{ad}$ -covered Co(0001) [10]. The decreases in  $E_{ad}$  for  $OH_x$  and  $CH_x$  species were lower compared to  $C_2H_2$ , CO and HCO, while sulfur only resulted in a slight reduction in  $E_{ad}$  of 4% for adsorbed H. These results point out that sulfur will result in increased H and decreased CO coverages on Co(111) combined with an increased coverage of OH and CH species, when compared to  $C_2$  molecules, such as  $C_2H_2$ .

In order to understand why sulfur induces relatively different changes in the adsorption energies of adsorbates, a Bader charge analysis was performed, the results of which are shown in Table 2.

**Table 2.** Total Bader charges on chemisorbed adsorbates on Co(111) vs. S-Co(111), together with changes in adsorption energies ( $E_{ad}$ ).

	Co(111)	S-Co(111)	$\Delta$ Charge (%)	$\Delta E_{ad}$ (%)
S	NA	-0.68	NA	NA
CO	-0.37 (top)	-0.54 (hcp)/-0.28 (top)	-25	-50
HCO	-0.73	-0.53	-27	-55
H	-0.41	-0.34	-16	-9
C	-0.88	-0.78	-11	-13
CH	-0.74	-0.62	-17	-6
$CH_2$	-0.64	-0.25	-62	-17
$CH_3$	-0.45	-0.20	-56	-49
$C_2H_2$	-0.95	-0.82	-14	-97
O	-1.03	-0.95	-8	-17
OH	-0.67	-0.60	-10	-25

Table 2 shows that sulfur withdraws electrons from the cobalt surface, as previously reported in surface science studies [10]. Based on this effect, the electronic charge decreases on all adsorbates investigated, when coadsorbed with atomic sulfur on Co(111). The decrease in electron density leads to decreases in  $E_{ad}$  for all adsorbates. For CO, the electronic charge appeared to increase from  $-0.37$  to  $-0.54$ , going from the top site on Co(111) to the hcp site on S-Co(111). However, if the Bader charge was analyzed for CO on the top site for S-Co(111), it was observed that there was a 22% decrease compared to CO on the top site for clean Co(111).

Table 2 also indicates that the magnitude of the decrease in total electronic density did not correlate with magnitude of the decrease in  $E_{ad}$  when comparing the distinct surface

species of H, CO, CH and OH. For example, relatively similar changes in electronic charge resulted in higher decreases for O(H) species compared to C(H). Among the different species, the  $E_{ad}$  for H and CH species were the least effected (9 to 13% decrease) by the decreases in charge, while O, OH, CO and HCO were influenced more with decreases in  $E_{ad}$  ranging from 17 to 55%. Similar results were obtained in a recent study that investigated the effect of Na<sub>2</sub>O on the charges and  $E_{ad}$  for H and CO on a Co(111) surface [35]. For the species of CO, CH<sub>2</sub> and CH<sub>3</sub>, the decrease in  $E_{ad}$  appeared to be more related to the change of adsorption site, as shown in Table 2 and Figure 1, compared to the electronic charge. C<sub>2</sub>H<sub>2</sub> species, for which the decrease in  $E_{ad}$  was the highest, occupied two adsorption sites, different than the other investigated adsorbates which occupied a single site. Therefore, the adsorption of C<sub>2</sub>H<sub>2</sub> is more sensitive to surface coverage, as discussed further in Section 3.3, where the effect of lower (<0.25 ML) sulfur coverages on the  $E_{ad}$  of adsorbates is investigated. These results show that the change in  $E_{ad}$  for different adsorbates involved in FTS is not simply a function of the electronic charge, but depends on the complex interplay of charges, adsorption sites and surface coverages.

### 3.2. Effect of Sulfur on the Elementary Reactions of FTS on Co(111)

#### 3.2.1. H-Assisted CO Dissociation

On cobalt particles, CO can dissociate via a direct or an H-assisted pathway. Experimentally, direct CO dissociation is not observed on both clean [36] and sulfur-poisoned [10] flat cobalt Co(0001) terraces. DFT calculations on both Co(0001) [37] and Co(111) [25] surfaces also indicate that direct CO dissociation is not likely to take place due to its significantly high activation barrier of >200 kJ/mol. Therefore, direct CO dissociation was not calculated in our investigation. For H-assisted CO dissociation, studies based on DFT calculations have indicated that COH formation is not favorable due to kinetic limitations on both Co(0001) [38] and Co(111) [25,39] surfaces. Therefore, as there is a consensus in the literature that H-assisted CO dissociation occurs via the HCO intermediate and not the COH intermediate, we investigated H-assisted CO dissociation via the HCO intermediate in our investigations.

Combined with our results showing an increased ratio of H/CO coverage on S-Co(111), only the H-assisted pathway was investigated in this study. A potential energy diagram (PED) for H-assisted CO dissociation on S-Co(111) is given in Figure 2.

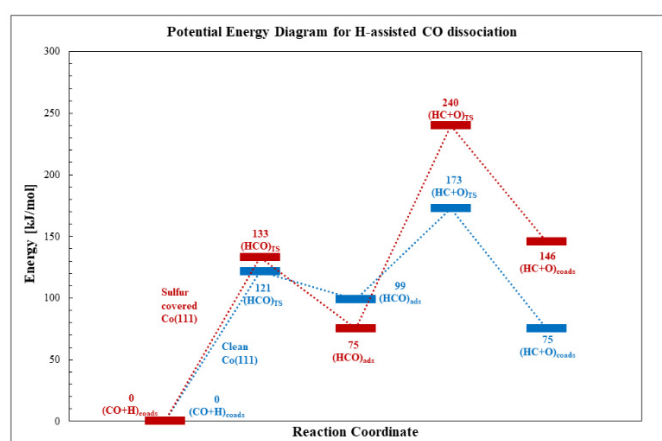


**Figure 2.** Potential energy diagram for H-assisted CO dissociation on Co(111) vs. S-Co(111).

Figure 2 shows that the activation barriers ( $E_a$ ) for formyl (HCO) formation and dissociation were increased on S-Co(111) by 12 and 91 kJ/mol, respectively. Furthermore, although the reaction energy (RE) for formyl formation remained relatively similar, for formyl dissociation, the reaction became endothermic with an RE of 71 kJ/mol compared to an exothermic dissociation on clean Co(111). These results show that sulfur inhibits H-assisted CO dissociation on Co(111) surfaces.

### 3.2.2. Oxygen Hydrogenation (Water Formation)

Oxygen hydrogenation can proceed through  $\text{OH}_x$  hydrogenation or OH coupling on the Co(111) surface. We investigated both of these pathways to determine the effects of  $\text{S}_{\text{ad}}$  on the activation barriers and reaction energies. Figure 3 shows the PED for water formation via  $\text{OH}_x$  hydrogenation while Figure 4 shows the PED for water formation via OH coupling.

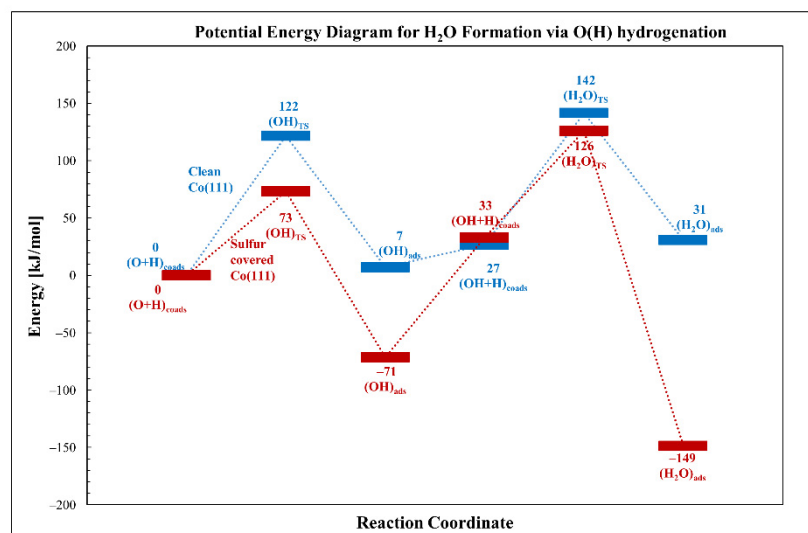


**Figure 3.** Potential energy diagram for water formation via  $\text{OH}_x$  hydrogenation on Co(111) vs. S-Co(111).

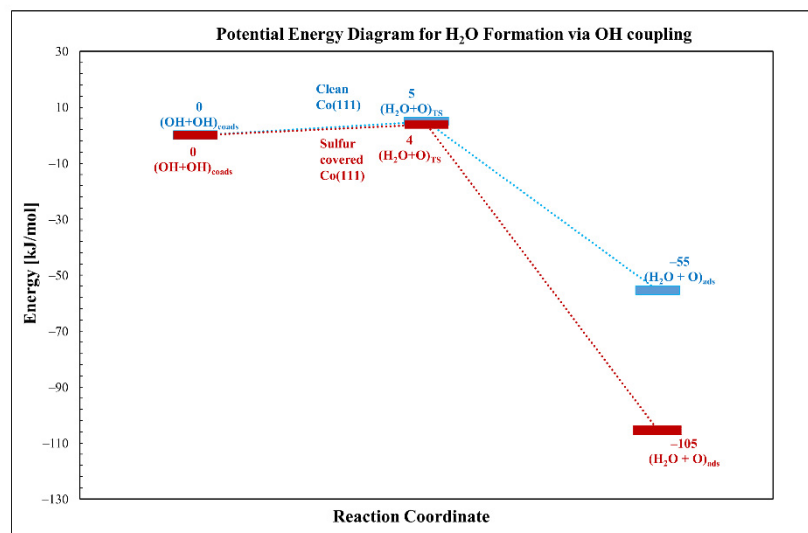


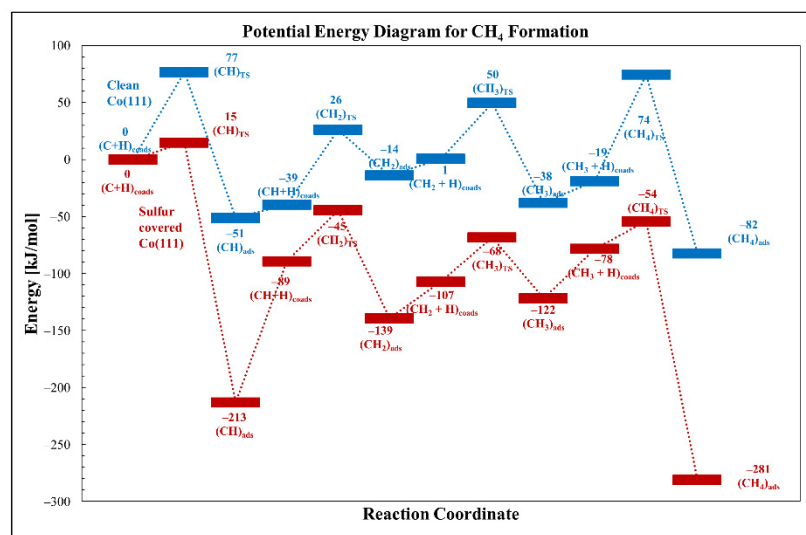
**Figure 4.** Potential energy diagram for water formation via OH coupling on Co(111) vs. S-Co(111).

Figures 3 and 4 show that sulfur decreased the activation barriers for  $\text{OH}_x$  hydrogenation and OH coupling pathways on Co(111) surfaces. In particular, the  $E_a$  for the formation of OH, the essential step in both pathways, was reduced by 49 kJ/mol, as seen in Figure 3. It has been previously reported that after OH formation, water formation via OH coupling is the preferred pathway due to its lower  $E_a$  compared to OH hydrogenation [40]. In the presence of sulfur, OH coupling is still the preferred pathway due to its lower barrier, and Figure 4 shows that the activation barrier for OH coupling was marginally lowered from 5 to 4 kJ/mol. Furthermore the reaction became more exothermic by 50 kJ/mol. Combining these results, it can be concluded that sulfur adsorption on Co(111) promotes the water formation reaction.

This conclusion is also in line with a previous computational investigation [40] which stated that Pt adsorbed on Co(111) reduces the charge transferred to adsorbates and therefore reduces the activation barriers for OH formation and OH coupling. Previously, it was proposed in the literature that water formation is a possible candidate for the rate limiting step of FTS [15,41]. Therefore, the calculations show that the poisoning effect of sulfur on Co(111) terraces is not due to inhibition of water formation, but instead stems from the lowering of the CO coverage due to a strong decrease in its adsorption energy and the inhibition of H-assisted CO dissociation due to a significant increase in the activation barrier for HCO dissociation.

### 3.2.3. Carbon Hydrogenation (Methane Formation)

As is indicated in Section 3.2.1, HCO dissociation that yields CH species is inhibited on Co(111) as a result of coadsorbed sulfur. The formation of atomic C on both Co(0001) [36] and sulfur-covered Co(0001) [10] is also not observed experimentally. However, as it has been mentioned that methane formation occurs on sulfur-covered Co(0001) surfaces [11], it may be proposed that the atomic carbon formed on defective/undercoordinated sites undergoes hydrogenation to methane on S-Co(111). It was also reported in the mentioned experimental report [11] that flat Co(0001) terraces covered with  $p(2 \times 2)$   $S_{ad}$  are surrounded by step/undercoordinated sites. Although it would be of interest to investigate how atomic carbon forms on these sites, this was beyond the scope of our study. Furthermore, as methane production has been shown to proceed on the terraces, indicated by the formation of a mixed S/C phase on the terraces after syngas exposure [11], the investigation of  $CH_4$  formation on S-Co(111) is necessary to understand the effects of sulfur on methane selectivity. The production of  $CH_4$  is well documented in the literature to proceed via the stepwise hydrogenation of atomic C species on Co(111) surfaces [33,42]. Therefore,  $CH_4$  formation via the stepwise hydrogenation of atomic C was investigated in our study. The PED for  $CH_4$  formation starting from adsorbed atomic carbon ( $C_{ad}$ ) is shown in Figure 5.



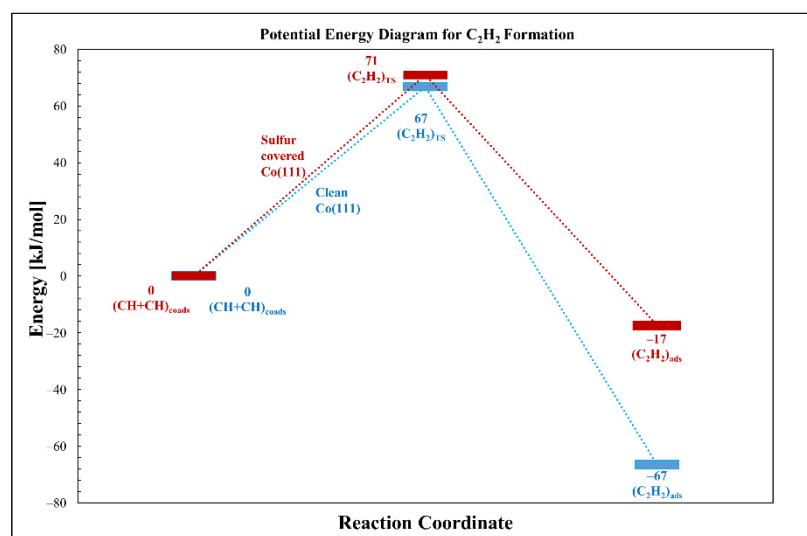
**Figure 5.** Potential energy diagram for methane formation on Co(111) vs. S-Co(111).

Figure 5 shows that the barriers for all  $CH_x$  hydrogenation steps were reduced, ranging from 10 to 69 kJ/mol. Therefore, the results indicate that sulfur significantly promotes the formation of  $CH_4$  on Co(111) surfaces. These results provide an explanation for the observed increase in methane selectivity in the recent experimental literature [6,7]. The decrease in the activation barriers could mainly stem from the higher destabilization of initial states in  $CH_x$  hydrogenation reactions, namely the coadsorption structures of S,  $CH_x$  and H on Co(111), compared to the final states of  $CH_x$  and S coadsorption, which results in increased exothermicity for all steps, with the exception of  $CH_3$  formation. The

destabilization was more pronounced for the  $\text{CH}_x$  and H coadsorptions on S-Co(111) because the presence of additional  $\text{H}_{\text{ad}}$  resulted in a higher surface coverage, pushing H atoms to the less stable top sites, as in the case of C-H coadsorption (Figure S6) and  $\text{CH}_x$  closer to  $\text{S}_{\text{ad}}$  and, as seen in CH-H coadsorption (Figure S7).

### 3.2.4. CH Coupling (Acetylene Formation)

Carbon coupling is an essential step in the FTS mechanism that results in the formation of carbon chains and the desired hydrocarbon products. The exact species that are involved and the mechanism for chain growth in FTS is a matter of ongoing debate. In a previous DFT investigation, it was reported that the  $\text{CH} + \text{HCO}$  reaction had a slightly lower barrier compared to  $\text{CH} + \text{CH}$  coupling [25], while in another DFT study, both  $\text{CH} + \text{HCO}$  and  $\text{CH} + \text{CH}$  coupling reactions were proposed to be among the most plausible three coupling pathways [43]. However, recent experimental studies on Co(0001) single crystals performed under a CO pressure of  $1 \times 10^{-7}$  mbar showed that CH, not HCO, is the coupling species, based on IR spectroscopy [44] and XPS [45] measurements. This result is also backed by observations on cobalt catalysts under applied FTS conditions [46,47]. Furthermore, our calculations indicate that sulfur decreased the adsorption energy of HCO significantly, while for CH species, the adsorption energy was not significantly affected. In addition, the presence of sulfur increased the activation barrier for HCO formation and promoted the decomposition of HCO back to H and CO species. These results indicate that for sulfur-covered Co(111) surfaces, HCO coverage would be significantly low compared to CH coverage. Therefore, in our study, we investigated CH coupling to form acetylene as a representative model reaction for chain growth in FTS on Co(111) surfaces. The PED for acetylene formation on Co(111) vs. S-Co(111) surfaces is shown in Figure 6.



**Figure 6.** Potential energy diagram for acetylene formation on Co(111) vs. S-Co(111) surfaces.

Figure 6 shows that sulfur caused a slight 4 kJ/mol increase in  $E_a$  for acetylene formation on Co(111). Although the increase was not pronounced, when comparing the CH coupling pathway with CH hydrogenation, it was observed that the barrier for CH hydrogenation was decreased while the barrier for CH coupling was increased. Furthermore, the significant drop in  $E_{\text{ad}}$  for  $\text{C}_2\text{H}_2$  implies that the formed  $\text{C}_2$  species will be more likely to desorb from the surface without having further chances for CH coupling reactions. This can be expected to result in the reduction in the chain growth rate on Co(111) surfaces.

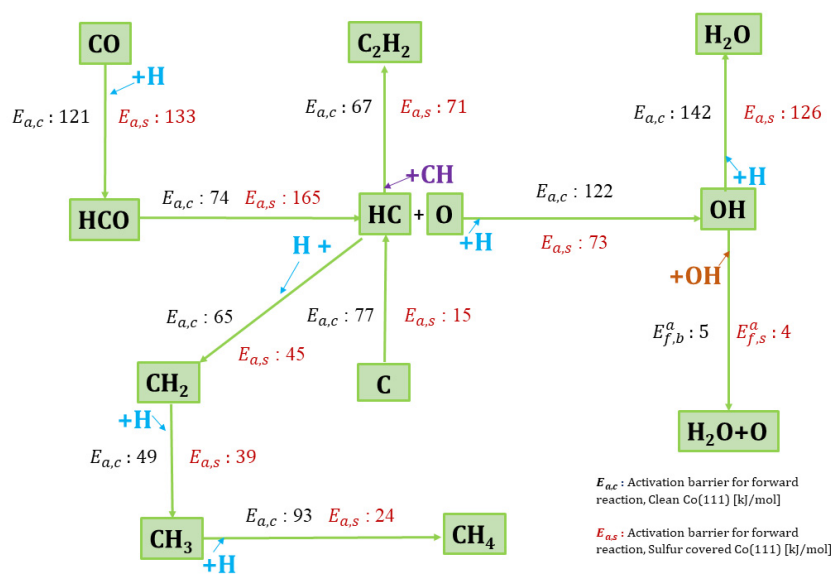
Table 3 summarizes the effect of  $\text{S}_{\text{ad}}$  on the activation barriers and reaction energies for the main elementary reactions of FTS on Co(111).

**Table 3.** Activation barriers ( $E_a$ ) and reaction energies (RE) for the main elementary reactions of FTS on Co(111) vs. S-Co(111).

	$E_a$		$\Delta E_a$	RE		$\Delta(\text{RE})$
	Co(111)	S-Co(111)		Co(111)	S-Co(111)	
H + CO → HCO	121	133	12	99	75	−24
HCO → HC + O	74	165	91	−24	71	95
C + H → CH	77	15	−62	−51	−214	−163
CH + H → CH <sub>2</sub>	65	45	−20	25	−50	−75
CH <sub>2</sub> + H → CH <sub>3</sub>	49	39	−10	−38	−15	23
CH <sub>3</sub> + H → CH <sub>4</sub>	93	24	−69	−64	−203	−139
CH + CH → C <sub>2</sub> H <sub>2</sub>	67	71	4	−67	−17	50
O + H → OH	122	73	−49	7	−71	−78
O + H → H <sub>2</sub> O	142	126	−16	31	−149	−180
OH + OH → H <sub>2</sub> O + O	5	4	−1	−55	−105	−50

The activation barriers obtained in this study match very well with the activation barriers obtained for HCO formation and dissociation [25], C(H) hydrogenation [25,33], O(H) hydrogenation and OH coupling [40] in the related literature, as shown in Table S2.

The reaction diagram summarizing the change in activation barriers for the main elementary reactions of FTS on Co(111) vs. S-Co(111) is shown in Figure 7.

**Figure 7.** Reaction diagram summarizing the effect of sulfur on the main elementary reactions of FTS on Co(111).

### 3.3. Effect of Sulfur Coverages Lower than 0.25 ML on FTS Adsorbates on Co(111)

It has been reported in the experimental literature that the effects of sulfur on cobalt-catalyzed FTS depend on sulfur coverage. Although it is difficult to measure the exact surface coverage on cobalt nanoparticles due to the ambiguities of surface structure, surface area and the amount of sulfur adsorbed, measurements based on activity loss coupled to ICP-MS data on sulfur adsorption have indicated that the sulfur coverage can increase up to around 0.6 ML, where the catalytic activity is completely lost [6,7]. In particular, above sulfur coverages of 0.1 ML [7] or 0.2 ML [6], the changes in selectivity become significant. Therefore, it is of interest how sulfur coverages lower than 0.25 ML effect FTS selectivity. To investigate these effects, the adsorption of key FTS reactants and intermediates were investigated at p(3 × 3) and p(4 × 4) periodic structures, corresponding to sulfur coverages of 0.11 ML and 0.06 ML, respectively. At these coverages, two different zones were formed

on the surface, with respect to their distance from the sulfur, with different adsorption sites, as shown in Figure 8.

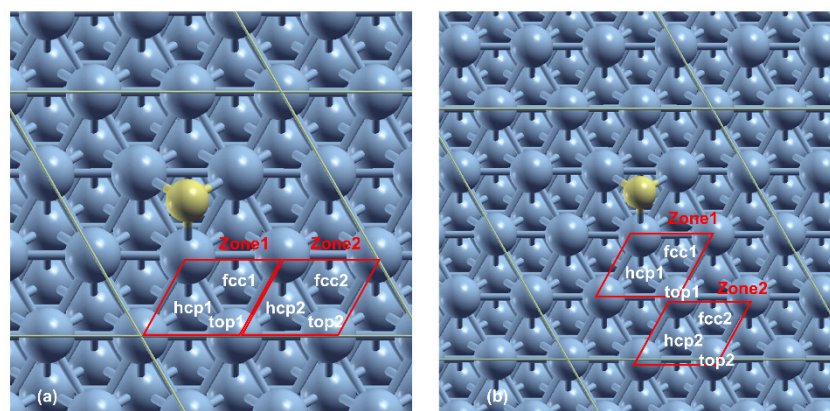


**Figure 8.**  $S_{ad}$  on Co(111) surfaces at (a) 0.11 ML and (b) 0.06 ML coverages, showing Zone1 (the zone closer to  $S_{ad}$ ) and Zone2 (the zone further away from  $S_{ad}$ ), with different hcp, fcc and top sites investigated in each zone (the bridge sites are not shown as no adsorbates converged to bridge sites after optimization).

The effects of sulfur on adsorption sites and energies are reported in detail in Table S3. It was observed that for both 0.11 ML and 0.06 ML surface coverages, for Zone2, sulfur did not affect the site preference for adsorbates, while its effects on  $E_{ad}$  were also negligible. These results are in line with observations on Ni(100) surfaces stating that the S-CO interactions are short ranged [1], and with the single crystal studies on Co(0001) surfaces indicating that the effect of 0.11 ML  $S_{ad}$  on the CO adsorption energy is minimal [10]. It is worthwhile to mention that even at these low sulfur coverages, the surface can be expected to have various surface species, including but not limited to  $CH_x$ ,  $OH_x$  and  $C_xH_y$  species, as indicated in previous experimental reports [15,16]. Therefore, it is highly probable that even at lower sulfur coverages under FTS conditions, the species can be forced to adsorb in close proximity to  $S_{ad}$  (i.e., Zone1 in our models) due to the repulsive interactions between species on a surface crowded with various adsorbates. For Zone1, where the adsorption sites are in close proximity to  $S_{ad}$ , it can be seen that the effects of sulfur are dependent on the type of adsorbate, as shown in Table 4.

**Table 4.** Relative changes in  $E_{ad}$  for adsorbates on Co(111) for various sulfur coverages.

	$\Delta E_{ad}$ (%)		
	$\theta_S = 0.25$ ML	$\theta_S = 0.11$ ML	$\theta_S = 0.06$ ML
CO	−50	−9	−9
H	−9	−4	−5
C	−13	−6	−4
CH	−6	−4	−4
$C_2H_2$	−97	−19	−10
O	−17	−8	−9
OH	−25	−8	−9

It can be seen that for all coverages, the relative decrease in  $E_{ad}$  was highest for  $C_2H_2$  and CO, while it was lowest for CH and H species. Furthermore, for CH and H, the decrease in  $E_{ad}$  did not change significantly as sulfur coverage was increased, while for CO and especially  $C_2H_2$ , the effect of  $S_{ad}$  was significantly dependent on coverage. In addition, for both 0.11 ML and 0.06 ML coverages, the adsorbates optimized at fcc1 sites converged, while CO diffused to top1 sites. This finding also illustrates that sulfur has a more pronounced site-blocking effect on CO compared to other species. The results

indicate that the coverage-dependent effects of sulfur on FTS selectivity may be related to the varying effects of sulfur on different species. These results are also in line with experimental findings stating that the effects of sulfur on selectivity are more pronounced for coverages higher than 0.2 ML [6], as  $S_{ad}$  coverages below 0.25 ML induce relatively small changes in  $E_{ad}$ . For the same reason, the activation barriers for the elementary reactions investigated in Table 3 were not calculated for coverages lower than 0.25 ML, as a major change in the activation barriers was not expected due to relatively low changes in  $E_{ad}$  for all species.

Therefore, the examination of Table 3 and Figure 7 can provide insights related to the effect of experimentally relevant (0.25 ML) sulfur coverages on the selectivity of FTS on Co(111) terraces. Sulfur results in major decreases in the activation barriers for CH hydrogenation, while increasing the exothermicity of these reactions simultaneously. However, for CH coupling, the activation barrier was slightly increased by 3 kJ/mol, while the reaction energy became more endothermic by 54 kJ/mol. These results indicate that sulfur would promote the formation of  $CH_4$ , while decreasing the selectivity to long-chain hydrocarbons. This effect is further amplified considering that the  $E_{ad}$  for  $C_2H_2$  decreased by 97% when co-adsorbed with sulfur. Under experimental conditions, these effects would result in the significant inhibition of chain formation on Co(111) terraces on surface sites close to  $S_{ad}$ . The effects of sulfur on selectivity can also be discussed from the perspective of CO and OH coverages on the Co(111) surface. It was previously reported that adsorbed CO [46,47] and OH [26] also promote the selectivity to heavier hydrocarbons via electronic effects. As sulfur decreases the adsorption energies (and as a result the coverages) of CO and OH more strongly compared to H and  $CH_x$ , this effect would also result in lower selectivity to heavier hydrocarbons and olefins compared to methane and saturated hydrocarbons. These findings compliment and provide a molecular understanding of recent experimental observations [6,7] related to the effect of sulfur on the selectivity of cobalt-catalyzed FTS. Although it is of interest to calculate the reaction kinetics based on DFT modelling, the calculation of kinetics necessitates assumptions about the surface coverage and the exact reaction mechanism that is responsible for the formation of various products. As the calculated reaction kinetics would depend on the reliability of these assumptions, the kinetics were not calculated in this manuscript. The comparison of the energetics of the investigated elementary reactions allowed us to qualitatively discuss the effects of sulfur on the selectivity of cobalt-catalyzed FTS, without the need to make assumptions about the surface coverages and exact reaction mechanism.

Overall, our results provide an explanation for the intrinsic effect of sulfur on metallic Co(111) terraces related to FTS selectivity. The results also show that such a computational surface science approach can be beneficial in generating insights related to experimentally controversial issues in heterogeneous catalysis, such as deactivation and promotion phenomena.

#### 4. Conclusions

The effect of sulfur on the selectivity of cobalt-catalyzed Fischer–Tropsch Synthesis was investigated by molecular modeling using density functional theory calculations. Based on the model of adsorbed atomic sulfur on Co(111) terraces for a sulfur coverage of 0.25 ML, the adsorption energies of surface species, including (H)CO,  $CH_x$ ,  $OH_x$  and  $C_2H_2$ , and the reaction parameters of elementary reactions—H-assisted CO dissociation, C hydrogenation for methane formation, O hydrogenation and OH coupling for water formation, and CH coupling for acetylene formation—were compared on clean Co(111) and sulfur-covered Co(111) surfaces. The effect of  $S_{ad}$  on adsorbates for sulfur coverages of 0.11 ML and 0.06 ML was also investigated. The following conclusions were drawn:

Sulfur poisoning of cobalt surfaces results in part from a reduction in CO coverage combined with the inhibition of (H)CO dissociation on flat cobalt surfaces.

For the experimentally observed  $p(2 \times 2)$  structure of sulfur, where sulfur coverage was 0.25 ML, the adsorbed atomic sulfur mainly inhibited the adsorption of CO, OH and

C<sub>2</sub>H<sub>2</sub> on cobalt surfaces, while the adsorption of H and CH species was not significantly affected. Furthermore, at 0.25 ML sulfur coverage, the activation barriers for OH and CH<sub>4</sub> formation were reduced, while the barriers for CH coupling and HCO dissociation were increased. It was also observed that for sulfur coverages of 0.11 ML and 0.06 ML, the effects of sulfur on C<sub>2</sub>H<sub>2</sub> and CO adsorption energies were the strongest, while its effects on CH and H adsorption energies were the weakest.

These findings indicate that sulfur modifies the selectivity mainly by increasing the surface H/CO ratio and by promoting CH<sub>4</sub> formation while inhibiting C-C coupling.

Therefore, sulfur poisoning on metallic cobalt surfaces is projected to lead to an increased selectivity to CH<sub>4</sub> and saturated light hydrocarbons and decreased selectivity to olefins and heavier hydrocarbons, supporting and explaining recent experimental findings.

**Supplementary Materials:** The following supporting information can be downloaded at: <https://www.mdpi.com/article/10.3390/catal12040425/s1>, Figure S1. Initial state (IS), transition state (TS) and final state (FS) for HCO formation (H+CO→HCO) on S-Co(111), Figure S2. Initial state (IS), transition state (TS) and final state (FS) for HCO dissociation (HCO→HC+O) on S-Co(111), Figure S3. Initial state (IS), transition state (TS) and final state (FS) for OH formation (O+H→OH+\*) on S-Co(111), Figure S4. Initial state (IS), transition state (TS) and final state (FS) for OH hydrogenation (OH+H→H<sub>2</sub>O+\*) on S-Co(111), Figure S5. Initial state (IS), transition state (TS) and final state (FS) for OH coupling (OH+OH→H<sub>2</sub>O+O) on S-Co(111), Figure S6. Initial state (IS), transition state (TS) and final state (FS) for CH formation (C+H→CH+\*) on S-Co(111), Figure S7. Initial state (IS), transition state (TS) and final state (FS) for CH<sub>2</sub> formation (CH+H→CH<sub>2</sub>+\*) on S-Co(111), Figure S8. Initial state (IS), transition state (TS) and final state (FS) for CH<sub>3</sub> formation (CH<sub>2</sub>+H→CH<sub>3</sub>+\*) on S-Co(111), Figure S9. Initial state (IS), transition state (TS) and final state (FS) for CH<sub>4</sub> formation (CH<sub>3</sub>+H→CH<sub>4</sub>+\*) on S-Co(111), Figure S10. Initial state (IS), transition state (TS) and final state (FS) for C<sub>2</sub>H<sub>2</sub> formation (CH+CH→C<sub>2</sub>H<sub>2</sub>+\*) on S-Co(111), Figure S11. Top and side views of S-Co(111) for 0.25 ML sulfur coverage, Table S1: Comparison of the calculated E<sub>ad</sub> with literature, Table S2. Comparison of the calculated activation barriers (E<sub>a</sub>) with literature, Table S3. E<sub>ad</sub> values for adsorbates for 0.25 ML, 0.11 ML and 0.06 ML adsorbate/sulfur coverages on Co(111)/S-Co(111).

**Author Contributions:** Conceptualization, A.C.K.; methodology, A.C.K.; validation, A.C.K.; formal analysis, A.C.K.; investigation, Y.D. and A.C.K.; resources, A.C.K.; data curation, A.C.K.; writing—original draft preparation, A.C.K.; writing—review and editing, A.C.K.; visualization, Y.D. and A.C.K.; supervision, A.C.K.; project administration, A.C.K. All authors have read and agreed to the published version of the manuscript.

**Funding:** This research received no external funding.

**Institutional Review Board Statement:** Not applicable.

**Informed Consent Statement:** Not applicable.

**Data Availability Statement:** The data presented in this study are available on request from the corresponding author.

**Acknowledgments:** The authors would like to thank the Izmir Institute of Technology for the computational time.

**Conflicts of Interest:** The authors declare no conflict of interest.

## References

1. Bartholomew, C.H. Mechanisms of catalyst deactivation. *Appl. Catal. A Gen.* **2001**, *212*, 17–60. [CrossRef]
2. Xie, J.; Paalanen, P.P.; van Deelen, T.W.; Weckhuysen, B.M.; Louwerse, M.J.; de Jong, K.P. Promoted cobalt metal catalysts suitable for the production of lower olefins from natural gas. *Nat. Commun.* **2019**, *10*, 1–10. [CrossRef]
3. Tsakoumis, N.E.; Ronning, M.; Borg, O.; Rytter, E.; Holmen, A. Deactivation of Cobalt Based Fischer-Tropsch Catalysts: A Review. *Catal. Today* **2010**, *154*, 162–182. Available online: <http://www.sciencedirect.com/science/article/pii/S0920586110002282> (accessed on 23 March 2022). [CrossRef]
4. Visconti, C.G.; Lietti, L.; Forzatti, P.; Zennaro, R. Fischer-Tropsch synthesis on sulphur poisoned Co/Al<sub>2</sub>O<sub>3</sub> catalyst. *Appl. Catal. A Gen.* **2007**, *330*, 49–56. [CrossRef]

5. Borg, Ø.; Hammer, N.; Enger, B.C.; Myrstad, R.; Lindvg, O.A.; Eri, S.; Skagseth, T.H.; Rytter, E. Effect of biomass-derived synthesis gas impurity elements on cobalt Fischer-Tropsch catalyst performance including in situ sulphur and nitrogen addition. *J. Catal.* **2011**, *279*, 163–173. [[CrossRef](#)]
6. Pansare, S.S.; Allison, J.D. An investigation of the effect of ultra-low concentrations of sulfur on a Co/ $\gamma$ -Al<sub>2</sub>O<sub>3</sub> Fischer-Tropsch synthesis catalyst. *Appl. Catal. A Gen.* **2010**, *387*, 224–230. [[CrossRef](#)]
7. Barrientos, J.; Montes, V.; Boutonnet, M.; Järås, S. Further insights into the effect of sulfur on the activity and selectivity of cobalt-based Fischer-Tropsch catalysts. *Catal. Today* **2016**, *275*, 119–126. [[CrossRef](#)]
8. Lahtinen, J.; Kantola, P.; Jaatinen, S.; Habermehl-Cwirzen, K.; Salo, P.; Vuorinen, J.; Lindroos, M.; Pussi, K.; Seitsonen, A.P. LEED and DFT investigation on the (2 × 2)-S overlayer on Co(0 0 1). *Surf. Sci.* **2005**, *599*, 113–121. [[CrossRef](#)]
9. Habermehl-Cwirzen, K.M.E.; Kauraala, K.; Lahtinen, J. Hydrogen on cobalt: The effects of carbon monoxide and sulphur additives on the D-2/Co(0001) system. *Phys. Scr. T* **2004**, *108*, 28–32. [[CrossRef](#)]
10. Habermehl-Cwirzen, K.; Lahtinen, J. Sulfur poisoning of the CO adsorption on Co(0001). *Surf. Sci.* **2004**, *573*, 183–190. [[CrossRef](#)]
11. Ehrensperger, M.; Wintterlin, J. In situ scanning tunneling microscopy of the poisoning of a Co(0001) Fischer-Tropsch model catalyst by sulfur. *J. Catal.* **2015**, *329*, 49–56. [[CrossRef](#)]
12. McAllister, B.; Hu, P. A density functional theory study of sulfur poisoning. *J. Chem. Phys.* **2005**, *122*, 084709. [[CrossRef](#)] [[PubMed](#)]
13. Curulla-Ferré, D.; Govender, A.; Bromfield, T.C.; Niemantsverdriet, J.W. A DFT study of the adsorption and dissociation of CO on sulfur-precovered Fe(100). *J. Phys. Chem. B* **2006**, *110*, 13897–13904. [[CrossRef](#)] [[PubMed](#)]
14. Ma, S.H.; Jiao, Z.Y.; Yang, Z.X. Coverage effects on the adsorption of sulfur on Co(0 0 1): A DFT study. *Surf. Sci.* **2010**, *604*, 817–823. [[CrossRef](#)]
15. Weststrate, C.J.; van Helden, P.; Niemantsverdriet, J.W. Reflections on the Fischer-Tropsch synthesis: Mechanistic issues from a surface science perspective. *Catal. Today* **2016**, *275*, 100–110. [[CrossRef](#)]
16. den Breejen, J.P.; Radstake, P.B.; Bezemer, G.L.; Bitter, J.H.; Frøseth, V.; Holmen, A.; de Jong, K.P. On the origin of the cobalt particle size effects in Fischer-Tropsch catalysis. *J. Am. Chem. Soc.* **2009**, *131*, 7197–7203. [[CrossRef](#)]
17. Kresse, G.; Hafner, J. Ab initio molecular dynamics for liquid metals. *Phys. Rev. B* **1993**, *47*, 558–561. [[CrossRef](#)]
18. Kresse, G.; Furthmüller, J. Efficient iterative schemes for ab initio total-energy calculations using a plane-wave basis set. *Phys. Rev. B* **1996**, *54*, 11169–11186. [[CrossRef](#)]
19. Zhang, Y.K.; Yang, W.T. Comment on “Generalized gradient approximation made simple”. *Phys. Rev. Lett.* **1998**, *80*, 890. [[CrossRef](#)]
20. Dion, M.; Rydberg, H.; Schroder, E.; Langreth, D.C.; Lundqvist, B.I. Van der Waals density functional for general geometries. *Phys. Rev. Lett.* **2004**, *92*, 246401. [[CrossRef](#)]
21. Roman-Perez, G.; Soler, J.M. Efficient Implementation of a van der Waals Density Functional: Application to Double-Wall Carbon Nanotubes. *Phys. Rev. Lett.* **2009**, *103*, 096102. [[CrossRef](#)] [[PubMed](#)]
22. Klimes, J.; Bowler, D.R.; Michaelides, A. Chemical accuracy for the van der Waals density functional. *J. Phys. Condens. Matter* **2010**, *22*, 022201. [[CrossRef](#)]
23. Klimes, J.; Bowler, D.R.; Michaelides, A. Van der Waals density functionals applied to solids. *Phys. Rev. B* **2011**, *83*, 195131. [[CrossRef](#)]
24. Gunasooriya, G.T.K.K.; van Bavel, A.P.; Kuipers, H.P.C.E.; Saeys, M. CO adsorption on cobalt: Prediction of stable surface phases. *Surf. Sci.* **2015**, *642*, L6–L10. [[CrossRef](#)]
25. Chen, C.; Wang, Q.; Wang, G.; Hou, B.; Jia, L.; Li, D. Mechanistic insight into the C<sub>2</sub> hydrocarbons formation from Syngas on fcc-Co(111) surface: A DFT study. *J. Phys. Chem. C* **2016**, *120*, 9132–9147. [[CrossRef](#)]
26. Gunasooriya, G.T.K.K.; van Bavel, A.P.; Kuipers, H.P.C.E.; Saeys, M. Key Role of Surface Hydroxyl Groups in C-O Activation during Fischer-Tropsch Synthesis. *ACS Catal.* **2016**, *6*, 3660–3664. [[CrossRef](#)]
27. Monkhorst, H.J.; Pack, J.D. Special Points for Brillouin-Zone Integrations. *Phys. Rev. B* **1976**, *13*, 5188–5192. [[CrossRef](#)]
28. Govender, A.; Curulla Ferré, D.; Niemantsverdriet, J.W. The surface chemistry of water on Fe(100): A density functional theory study. *ChemPhysChem* **2012**, *13*, 1583–1590. [[CrossRef](#)]
29. Henkelman, G.; Arnaldsson, A.; Jónsson, H. A fast and robust algorithm for Bader decomposition of charge density. *Comput. Mater. Sci.* **2006**, *36*, 354–360. [[CrossRef](#)]
30. Sanville, E.; Kenny, S.D.; Smith, R.; Henkelman, G. Improved grid-based algorithm for Bader charge allocation. *J. Comput. Chem.* **2007**, *28*, 899–908. [[CrossRef](#)]
31. Tang, W.; Sanville, E.; Henkelman, G. A grid-based Bader analysis algorithm without lattice bias. *J. Phys. Condens. Matter.* **2009**, *21*, 084204. [[CrossRef](#)] [[PubMed](#)]
32. Henkelman, G.; Uberuaga, B.P.; Jonsson, H. A climbing image nudged elastic band method for finding saddle points and minimum energy paths. *J. Chem. Phys.* **2000**, *113*, 9901–9904. [[CrossRef](#)]
33. Pedersen, E.Ø.; Svenum, I.H.; Blekkan, E.A. Mn promoted Co catalysts for Fischer-Tropsch production of light olefins—An experimental and theoretical study. *J. Catal.* **2018**, *361*, 23–32. [[CrossRef](#)]
34. Balakrishnan, N.; Joseph, B.; Bhethanabotla, V.R. Effect of platinum promoters on the removal of O from the surface of cobalt catalysts: A DFT study. *Surf. Sci.* **2012**, *606*, 634–643. [[CrossRef](#)]

35. Jeske, K.; Kizilkaya, A.C.; López-Luque, I.; Pfänder, N.; Bartsch, M.; Concepción, P.; Prieto, G. Design of Cobalt Fischer-Tropsch Catalysts for the Combined Production of Liquid Fuels and Olefin Chemicals from Hydrogen-Rich Syngas. *ACS Catal.* **2021**, *11*, 4784–4798. [[CrossRef](#)] [[PubMed](#)]
36. Weststrate, C.J.; van de Loosdrecht, J.; Niemantsverdriet, J.W. Spectroscopic insights into cobalt-catalyzed Fischer-Tropsch synthesis: A review of the carbon monoxide interaction with single crystalline surfaces of cobalt. *J. Catal.* **2016**, *342*, 1–16. [[CrossRef](#)]
37. Zhuo, M.K.; Tan, K.F.; Borgna, A.; Saeys, M. Density Functional Theory Study of the CO Insertion Mechanism for Fischer-Tropsch Synthesis over Co Catalysts. *J. Phys. Chem. C* **2009**, *113*, 8357–8365. [[CrossRef](#)]
38. Ojeda, M.; Nabar, R.; Nilekar, A.U.; Ishikawa, A.; Mavrikakis, M.; Iglesia, E. CO activation pathways and the mechanism of Fischer-Tropsch synthesis. *J. Catal.* **2010**, *272*, 287–297. [[CrossRef](#)]
39. Qi, Y.; Yang, J.; Chen, D.; Holmen, A. Recent Progresses in Understanding of Co-Based Fischer-Tropsch Catalysis by Means of Transient Kinetic Studies and Theoretical Analysis. *Catal. Lett.* **2015**, *145*, 145–161. [[CrossRef](#)]
40. Govender, S.; Gambu, T.G.; van Heerden, T.; van Steen, E. Mechanistic pathways for oxygen removal on Pt-doped Co(111) in the Fischer-Tropsch reaction. *Catal. Today* **2020**, *342*, 142–151. [[CrossRef](#)]
41. Kizilkaya, A.C.; Niemantsverdriet, J.W.; Weststrate, C.J. Oxygen Adsorption and Water Formation on Co(0001). *J. Phys. Chem. C* **2016**, *120*, 4833–4842. [[CrossRef](#)]
42. Chen, W.; Pilot, I.A.W.; Pestman, R.; Hensen, E.J.M. Mechanism of Cobalt-Catalyzed CO Hydrogenation: 2. Fischer-Tropsch Synthesis. *ACS Catal.* **2017**, *7*, 8061–8071. [[CrossRef](#)]
43. Qi, Y.; Yang, J.; Holmen, A.; Chen, D. Investigation of C1 + C1 coupling reactions in cobalt-catalyzed fischer-tropsch synthesis by a combined dft and kinetic isotope study. *Catalysts* **2019**, *9*, 551. [[CrossRef](#)]
44. Weststrate, C.J.; Niemantsverdriet, J.W. CO as a Promoting Spectator Species of C<sub>x</sub>H<sub>y</sub> Conversions Relevant for Fischer-Tropsch Chain Growth on Cobalt: Evidence from Temperature-Programmed Reaction and Reflection Absorption Infrared Spectroscopy. *ACS Catal.* **2018**, *8*, 10826–10835. [[CrossRef](#)]
45. Weststrate, C.J.; Sharma, D.; Rodriguez, D.G.; Gleeson, M.A.; Fredriksson, H.O.A.; Niemantsverdriet, J.W. Mechanistic insight into carbon-carbon bond formation on cobalt under simulated Fischer-Tropsch synthesis conditions. *Nat. Commun.* **2020**, *11*, 1–10. [[CrossRef](#)] [[PubMed](#)]
46. Rytter, E.; Holmen, A. Perspectives on the Effect of Water in Cobalt Fischer-Tropsch Synthesis. *ACS Catal.* **2017**, *7*, 5321–5328. [[CrossRef](#)]
47. Rytter, E.; Borg, Ø.; Tsakoumis, N.E.; Holmen, A. Water as key to activity and selectivity in Co Fischer-Tropsch synthesis:  $\Gamma$ -alumina based structure-performance relationships. *J. Catal.* **2018**, *365*, 334–343. [[CrossRef](#)]